Microwave-excited atmospheric-pressure microplasmas based on a coaxial transmission line resonator

2009 Plasma Sources Sci. Technol. 18 025029

(http://iopscience.iop.org/0963-0252/18/2/025029)

Plasma Sources Sci. Technol. **18** (2009) 025029 (8pp) doi:10.1088/0963-0252/18/2/025029

Microwave-excited atmospheric-pressure microplasmas based on a coaxial transmission line resonator

J Choi[1], F Iza[2], H J Do[3], J K Lee[1] and M H Cho[3]

[1] Department of Electronic and Electrical Engineering, Pohang University of Science and Technology, Pohang 790-784, Korea
[2] Department of Electronic and Electrical Engineering, Loughborough University, Loughborough, Leicestershire LE11 3TU, UK
[3] Department of Physics, Pohang University of Science and Technology, Pohang 790-784, Korea

E-mail: jkl@postech.ac.kr

Received 28 October 2008, in final form 10 February 2009
Published 31 March 2009
Online at stacks.iop.org/PSST/18/025029

Abstract
We report the design, fabrication and characterization of two microwave-excited microplasma sources based on coaxial transmission line resonators (CTLR). The sources are capable of generating electric fields of $\sim 10^6$ V m^{-1} at 900 MHz and 2.45 GHz. These devices can self-ignite helium or argon discharges in a wide pressure range including atmospheric pressure. The gas temperature in an argon discharge open to atmospheric air is ~400 K. Using air as a dielectric, the working gases can be passed through the CTLR, resulting in the formation of plasma jets suitable for surface treatments. The device efficiency on transferring the input power into the plasma is 50–85% depending on the gas used. No thermal damage or electrode erosion has been observed in the devices.

(Some figures in this article are in colour only in the electronic version)

1. Introduction

Portable plasma sources for generation of low-power atmospheric-pressure microplasmas are in increasing demand. A number of plasma sources with various electrode configurations have been developed [1]. Sources operating with dc [2, 3], low-frequency (kHz) [4], rf [5–7], microwave [8–10] and pulsed [11] power have been reported. Microwave-induced atmospheric-pressure plasmas have been used for analytical purposes [10], surface modification and biomedical applications such as cell treatment, sterilization [12] and decontamination of toxic agents [13–15].

Microwave-induced microplasmas can possibly meet the need for long-lifetime devices capable of operating at atmospheric pressure [16]. In these devices the energy of the ions striking the electrodes is very low due to the collisional nature of the sheath [17–19] and the low sheath potential that develops at high frequency [8, 16, 20]. Furthermore, with the rapid increase in telecommunication applications a variety of low-cost integrated circuits (ICs) are available for the design of a suitable power source, making possible the construction of a compact low-cost plasma generator that operates at microwave frequencies.

In this paper, a new portable microplasma source based on a coaxial transmission line resonator (CTLR) is described. The design and performance of the device is parallel to that of microstrip based devices [8, 9, 16] but this device has a pen-like shape that makes it more convenient for hand-held applications and parallel operation, or both. Unlike the coaxial device reported in [10], the device presented in this paper operates at resonance, resulting in an efficient plasma source. Furthermore, because the device operates at resonance, the input impedance of the device is real and a feeding point where the input impedance is 50 Ω can be found along the resonator. This eliminates the need for a matching network, resulting in a compact and efficient device.

Two devices are reported in the paper. One operates at ~2.45 GHz and uses a Teflon-based dielectric. The other operates at ~900 MHz and uses air as a dielectric; using air eliminates dielectric losses and allows the flow of gases

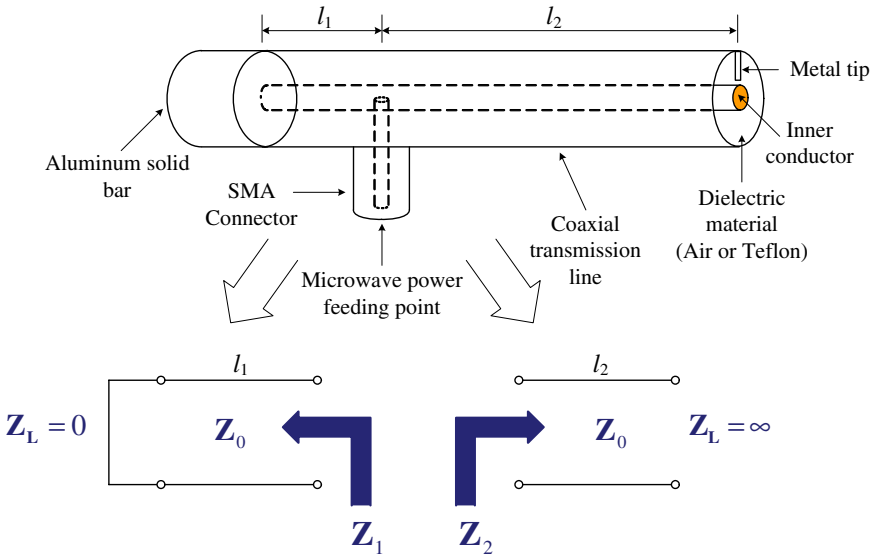

Figure 1. The schematic of the CTLR and the simplified microwave model.

through the device, which in turn allows the plasma chemistry to be adjusted to specific applications. In this paper, both devices are characterized by means of electrical and optical diagnostics. Argon and helium atmospheric discharges have been sustained with power efficiencies (i.e. the power coupled to the plasma divided by the total power delivered by the microwave power source) of ∼55% and ∼85%, respectively. The discharges are not in thermal equilibrium and the rotational temperature of OH molecules in the discharge is ∼400 K. This temperature decreases as one moves to the afterglow and the surface temperature on the open end of the CTLR is well below ∼60 °C.

2. Design of the CTLR plasma source

The CTLR plasma source consists of a coaxial transmission line in which one end is short-circuited and the other end is open (figure 1). To cause the transmission line to resonate at the excitation frequency, the length L of this line is chosen to be an odd number of quarter wavelengths. At resonance, the highest electric field is obtained at the open end of the device where the plasma is to be ignited. Depending on the input power and the quality of the resonator, the electric field at the open end can reach values high enough to self-ignite a plasma without using external igniters. The overall operation principle and design procedure are similar to those used in the microstrip split-ring resonator plasma source [8, 16]. To enhance the electric field at the open end of the device a small 'metal tip' is used (figure 1). This tip increases the electric field by decreasing the distance between the powered (inner) and grounded (outer) electrodes without significantly affecting the overall behavior of the resonator.

The power is coupled into the device through a subminiature type A (SMA) connector that is located at a point where the input impedance to the device is 50 Ω, eliminating the need for matching networks and the power losses associated with them. The input impedance to the device depends on the location of the input port; it is given by the parallel contribution of a shorted transmission line and an open transmission line (equation (1)):

$$\begin{aligned} Z_{\text{in}} = Z_1 || Z_2 &= Z_0 \left[\frac{1}{\tanh(jkl_1)} + \tanh(jkl_2) \right]^{-1} \\ &\approx Z_0 \Bigg[\left(\frac{\alpha l_1}{\sin^2(\beta l_1)} + \frac{\alpha l_2}{\cos^2(\beta l_2)} \right) \\ &\quad + \mathrm{j} \left(-\cot(\beta l_1) + \tan(\beta l_2) \right) \Bigg]^{-1}, \end{aligned} \tag{1}$$

where Z_0 is the characteristic impedance of the coaxial transmission line, $\mathrm{j} = \sqrt{-1}$, l_1 is the distance from the feeding point to the short-circuited port, l_2 is the distance from the feeding point to the open port, α is the attenuation constant, $\beta = 2\pi/\lambda$ is the phase constant of the coaxial line and $k = \beta - \mathrm{j}\alpha$ is the complex propagation constant or wave number [21]. In deriving the approximate final result in equation (1), we assume that $\alpha l \ll 1$, i.e. that the transmission line has small losses, and therefore $\tan(\alpha l) \cong \alpha l$. At resonance, $l_1 + l_2 = (2n-1)\lambda/4$, $n = 1, 2, 3, \ldots$, and the imaginary part of the input impedance vanishes, i.e. $\tan(\beta l_2) - \cot(\beta l_1) = 0$. Therefore, the input impedance of the resonator Z_{in} is real and its value can be controlled by adjusting the location of the input port (and consequently, the value of l_1).

The voltage at the open end can be estimated as follows. For a given input power P_{in} the voltage at the input port is given by

$$V_{\text{in}} = V(l_1) = \sqrt{2 P_{\text{in}} Z_{\text{in}}}, \tag{2}$$

and because the device operates at resonance, the voltage distribution along the resonator is

$$V(x) = V_{\text{gap}} \sin\left(\frac{x}{L} \frac{\pi}{2} \right), \tag{3}$$

i.e. a sinusoidal function with $V(0) = 0$ at the short end and $V(L) = V_{\text{gap}}$ at the open end. Combining equations (2) and

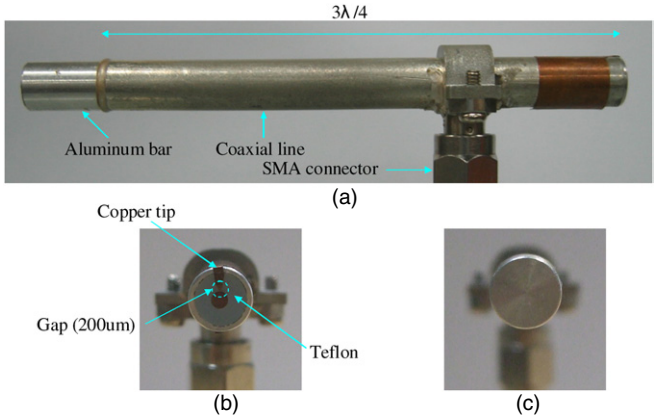

Figure 2. Device I: CTLR for operation at ∼2.45 GHz. (*a*) Side, (*b*) front and (*c*) rear view.

(3) shows that the voltage at the open end as a function of the input power is given by

$$V_{\text{gap}} = 2\sqrt{2\frac{Z_0 Q P_{\text{in}}}{\pi}}, \tag{4}$$

where $Q = \pi/(\alpha\lambda)$ is the quality factor of the resonator [16, 21]. Therefore, to generate a high electric field (high voltage across the gap) at a given input power level, $Z_0 Q$ should be maximized (characteristic impedance and quality factor should both be high). For a given input power, the gap voltage in the CTLR devices is $1/\sqrt{2}$ times that in a microstrip split-ring resonator device [16]. This difference occurs because the ring structure of the latter amplifies the voltage across the discharge gap because the two ends of the resonator face each other.

Equations (1) and (4) guided the design of the devices reported in this paper. Final tuning regarding the influence of fringing fields, perturbations introduced by the SMA connector and the impact of the metal tip on the resonator was achieved using computer simulations in the High Frequency Structure Simulator (HFSS, Ansoft Corporation).

3. Device fabrication and experimental setup

Two devices are reported in this paper; both were designed based on the procedure detailed in section 2. The first device (device I, figure 2) was designed to operate at 2.45 GHz. It was built using a commercial semi-rigid 50 Ω coaxial line (Micro-Coax, UT 250). The inner conductor, dielectric material and outer conductor are made of copper, Teflon and aluminum, respectively. The dielectric constant ε_r of Teflon is 2.1 and therefore at 2.45 GHz, $\lambda/4 \cong 2$ cm and a 50 Ω matched input port in a quarter-wavelength resonator should be located at $l_1 = 0.5$ mm from the short-circuited port. For convenience, therefore, device I was made $3\lambda/4$ long, $l_1 = 20$ mm and $l_2 = 45$ mm ($l_1 + l_2 = 65$ mm). A high-performance SMA connector (PSF-S03-000-2cc, Gigalane Co.) is used to feed the CTLR and silver paste is applied around the connection to minimize leakage of microwave power. An aluminum solid bar and silver epoxy are used to short circuit the resonator at the shorted end and a copper metal tip is used at the open end to enhance the electric field between the inner and outer conductors of the coaxial line. The gap between the metal tip and the inner conductor is 200 μm (table 1).

Table 1. The details and comparison of devices I and II.

	Device I	Device II
Frequency	2.436 GHz	875 MHz
Characteristic impedance (Z_0)	50 Ω	50 Ω
Dielectric Material	PTFE (Teflon)	Air
Quality factor (Q)	265	69.7
Gap distance	200 μm	40 μm
Gas flow	NOT Possible	Possible
Overall length ($l_1 + l_2$)	65 mm	83.5 mm
l_1	20 mm	6 mm
l_2	45 mm	77.5 mm

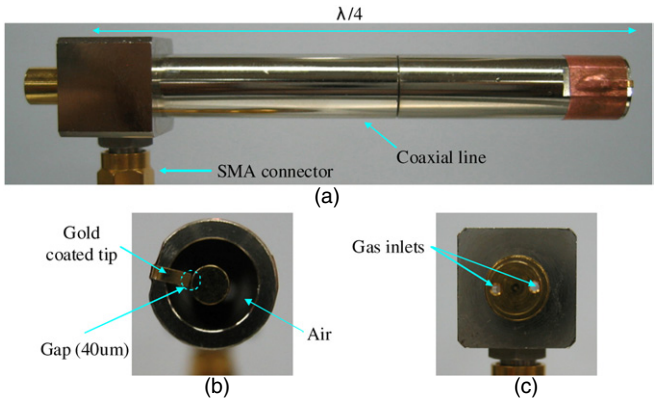

Figure 3. Device II: CTLR for operation at ∼900 MHz. (*a*) Side, (*b*) front and (*c*) rear view.

Device II was designed to operate at 900 MHz and used air as a dielectric (figure 3). Because the operation frequency is lower than that of device I and the wavelength longer, the CTLR of device II is only $\lambda/4$ long. According to equation (1), the input port should be located at $l_1 = 2.3$ mm, but this was modified as a result of HFSS simulations to 2.5 mm. The characteristic impedance of the coaxial line is 50 Ω. A gold coated tip was soldered at the open end to reduce locally the discharge gap to 40 μm. The inner and outer conductors of the coaxial line are made of brass and the inner and outer conductors of SMA connector are made of beryllium copper (BeCu) and stainless steel, respectively. Unlike device I, the aluminum bar used in device II to short circuit one of the ends of the CTLR has two holes through which gas can flow into the coaxial line. In device II, $l_1 = 6$ mm and $l_2 = 77.5$ mm ($l_1 + l_2 = 83.5$ mm) (table 1). Flowing gas at a sufficiently high flow rate results in the formation of a plasma jet at the open end of the plasma source.

The actual resonant frequencies of the devices as measured with a network analyzer were 2.43 GHz for device I and 875 MHz for device II. The deviation from the intended 2.45 GHz and 900 MHz is attributed to deviation in the actual material properties used in the design of the devices and to fabrication imprecision. Future designs can correct for these deviations by adjusting the length of the devices based on this first experience. The devices were tested in a cylindrical quartz vacuum chamber. The chamber was pumped down by a mechanical pump (Alcatel Drytel 31) and

filled back with either helium, argon or air as required by the experiment. The pressure inside the chamber was monitored by convection and bourdon gauges. The plasma sources were powered by a signal generator (HP 83640B) and a microwave power amplifier (AR 60S1G3). The forward and reflected powers were simultaneously monitored with two directional couplers (Narda 3202B-20), two sets of power sensors (Agilent N1921A, HP 8482A) and power meters (Agilent N1911A, HP EPM-441A).

The devices were also operated in open air, and the optical emission spectra of the discharges were measured using a spectrometer (DongWoo Optron DM750i) including a high sensitivity of photomultiplier tube (PMT, R928 Hamamatsu) and a detector assembly (DongWoo Optron PDS-1).

4. Experimental results and discussion

4.1. Discharge breakdown

When the device was powered, a high electric field developed at the open end of the resonator. This electric field was further enhanced by the metal tip that is added to locally reduce the gap between the powered center electrode and the external ground electrode. This high electric field allows the ignition of the discharge up to atmospheric pressure without using an external igniter. The ignition power was measured by slowly increasing the input power into the device and recording the power just before the discharge ignited. The ignition power was measured at least three times under each combination of conditions. When the discharge ignited, the impedance of the gap changed abruptly and so did the reflected power. In this work, we report input power to the device as the difference between the forward and reflected power.

The power required to ignite the discharge decreased as the pressure was reduced (figure 4). A minimum ignition power occurred at ∼1 Torr, and this is attributed to the maximum energy transfer to the electrons when the rf excitation frequency ω_{rf} approaches the electron neutral collision frequency ν [16, 22]. As a result, when the rf frequency decreased from 2.45 GHz (device I) to 900 MHz (device II), the minimum in the ignition power curve shifted towards lower pressures (figures 4(*a*) and (*b*)). Both devices can ignite helium atmospheric-pressure discharges with ∼0.75 W, power that can be delivered with-off-the-shelf IC amplifiers used in telecommunication applications.

The CTLR plasma source can ignite discharges without using an external igniter in a wide pressure range, including low-pressure conditions in which the electron mean free path λ_e is larger than the gap size. As in microstrip split-ring resonators, this is possible because of the coplanar structure of the electrodes [23, 24]. The electric field lines across the gap are not all of the same length. At low pressure, electrons can follow paths longer than the gap size at which the collisionality is sufficient to start the discharge. Therefore, a small gap size is important in starting the discharge at high pressures because it provides a region of high electric field. At lower pressures, however, the discharge is ignited by the electric field outside the gap, because this field provides longer paths and

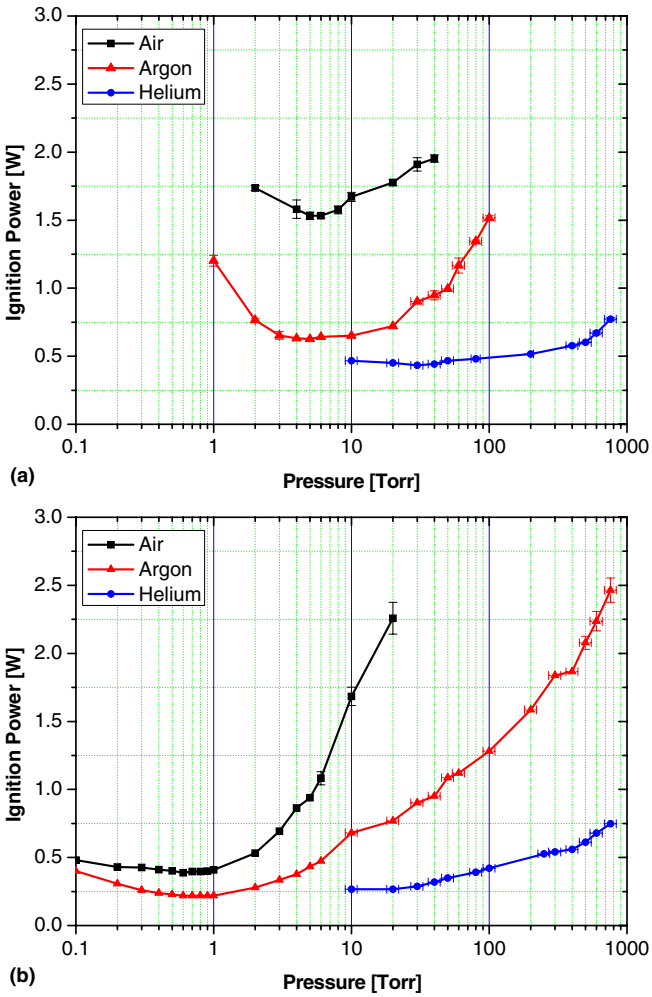

Figure 4. Ignition power in air, argon and helium of two devices: (*a*) device I (∼2.45 GHz) and (*b*) device II (∼900 MHz).

therefore lowers the electron drift loss. Although the electric field outside the gap is less intense than within the gap, this is compensated in part by better power transfer from the electric field to the electrons as pressure is reduced.

Using equation (4), the discharge breakdown voltage can be estimated from the measured ignition power (figure 5). As observed in other microwave breakdown studies [16, 25], the breakdown voltage for both devices is lower than the dc breakdown voltage.

4.2. Description of the discharge

Once the discharge is ignited, the discharge appearance depends on the operation pressure (figure 6). At low pressure, the plasma expanded out of the gap creating a uniform glow that covered the whole diameter of the device (figure 6(*a*)). As the pressure was increased, the mean free path of the particles decreased and the plasma became confined closer to the region where the electrons were being heated (figure 6(*b*)). At atmospheric pressure the discharge was confined to the tip region, creating an intense glow-like discharge. This observation agrees with those made using an argon plasma sustained by a microstrip split-ring resonator [8, 26]. Here as well, no indication of thermal damage or erosion was observed.

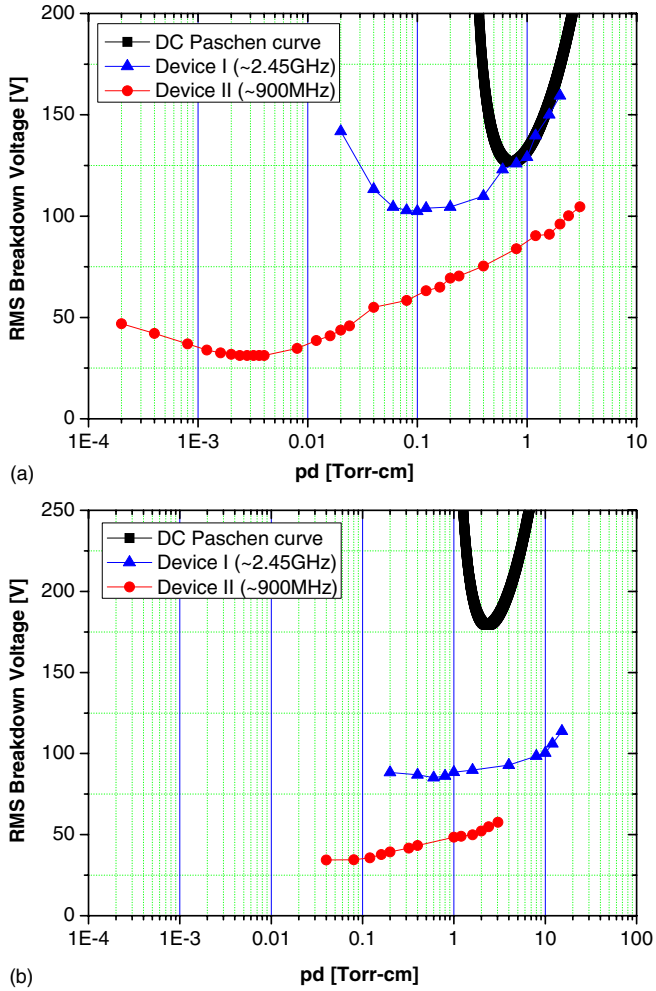

Figure 5. Comparison between theoretical dc Paschen curve and the microwave breakdown voltage of devices I and II. (*a*) Argon and (*b*) helium.

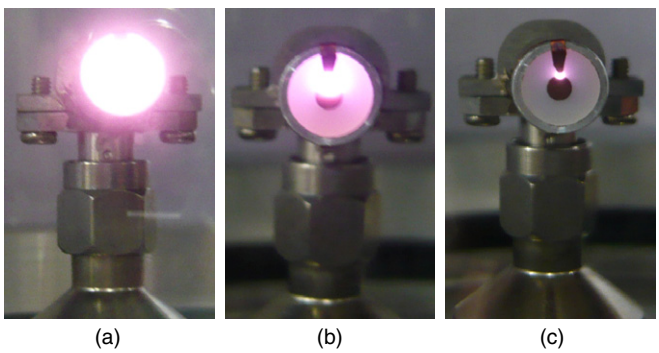

Figure 6. Helium microplasmas sustained with 0.3 W of device I: 10, 100 and 760 Torr (from (*a*) to (*c*)).

Although discharges can be sustained in the absence of gas flow, it is of interest in the formation of a plasma jet to facilitate the application of the plasma treatment. This can be readily done with device II by flowing gas through the CTLR. A 7 mm argon microwave-induced microplasma jet can be generated at 2 standard liters per minute (slm) gas flow rate and 2.5 W input power (figure 7).

Figure 7. Argon microplasma jet of device II with 2.5 W input power and 2 slm flow rate at atmospheric pressure.

4.3. Plasma impedance

Based on transmission line theory the plasma impedance at the tip of the resonator can be determined by measuring the reflection coefficient (s_{11}) [16]. In the presence of plasma, the input impedance Z_{in} of the resonator is the parallel combination of a shorted transmission line of length l_1 and an open transmission line of length l_2 terminated by a plasma impedance Z_{p}:

$$Z_{\text{in}} = Z_0 \left[\frac{1}{\tanh(\text{j}kl_1)} + \frac{Z_0 + Z_{\text{p}} \tan(\text{j}kl_2)}{Z_{\text{p}} + Z_0 \tan(\text{j}kl_2)} \right]^{-1}. \quad (5)$$

Therefore, the reflection coefficient of the plasma source when the plasma is present is given by

$$\begin{aligned} S_{11} &= \frac{Z_{\text{in}} - Z_{\text{ref}}}{Z_{\text{in}} + Z_{\text{ref}}} \\ &= \left[Z_0 - Z_{\text{ref}} \left(\frac{1}{\tanh(\text{j}kl_1)} + \frac{Z_0 + Z_{\text{p}} \tan(\text{j}kl_2)}{Z_{\text{p}} + Z_0 \tan(\text{j}kl_2)} \right) \right] \\ &\quad \times \left[Z_0 + Z_{\text{ref}} \left(\frac{1}{\tanh(\text{j}kl_1)} + \frac{Z_0 + Z_{\text{p}} \tan(\text{j}kl_2)}{Z_{\text{p}} + Z_0 \tan(\text{j}kl_2)} \right) \right]^{-1}, \end{aligned} \quad (6)$$

where $Z_{\text{ref}} = 50\,\Omega$ is the impedance of the power supply. Because we can measure the forward and reflected power at various frequencies, Z_{p} can be determined by fitting the experimental data with equation (6) [16] (figure 8). In the presence of plasma, the resonant frequency shifts towards lower frequencies due to the capacitive loading of the resonator and the quality factor decreases due to the power dissipation in the plasma. As in [16], the plasma impedance is dominated by the resistive component. This contrasts with conventional low-pressure discharges in which the capacitive nature of the sheath dominates the plasma impedance.

Assuming the discharge geometry as a bridge 40 μm long ($L_{\text{bulk}} = 40\,\mu\text{m}$) with a cross section A_{bulk} of $1.5 \times 3\,\text{mm}^2$, a gas temperature T_{g} of 400 K and an electron temperature T_{e} of ~1 eV, the mean bulk plasma density for a 0.8 W argon discharge at atmospheric pressure was estimated to be $n_{\text{e}} = (L_{\text{bulk}} m_{\text{e}} \nu)/(R_{\text{p}} q^2 A_{\text{bulk}}) \sim 4 \times 10^{14}\,\text{cm}^{-3}$ [22]. Here q is the elementary charge, m_{e} the mass of the electron, ν the electron collision frequency and R_{p} the real part of the plasma impedance (~775 Ω). The resulting plasma density is of the same order as the one reported in similar devices [16, 29]. In addition, the electron density was also estimated by measuring a fringe shift based on the Mach–Zehnder interferometer method [30]. At 1 W input power, the result is $1.1 \times 10^{14}\,\text{cm}^{-3}$, which is on the same order of the estimation using the plasma impedance.

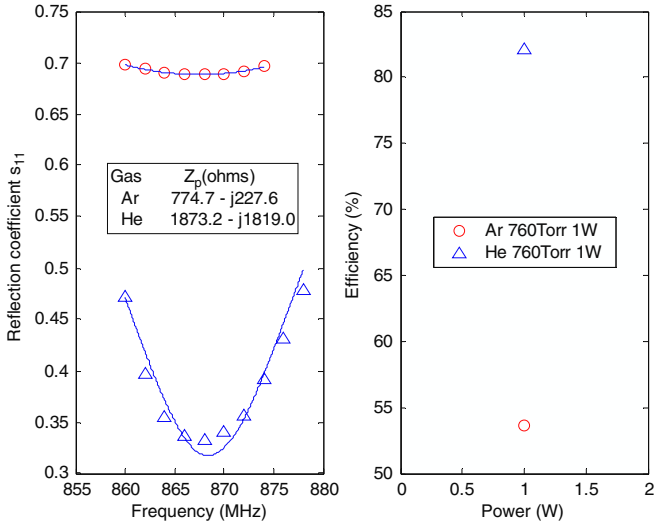

Figure 8. Plasma impedance and power efficiency of argon and helium microplasmas at atmospheric pressure with device II.

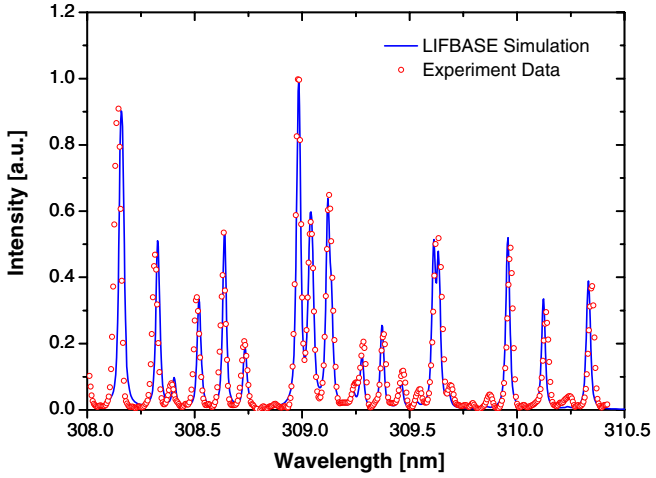

Figure 9. The rotational temperature estimation (400 K) of device II at 1.5 W input power and 15 slm gas flow rate at atmospheric pressure of the OH band based on LIFBASE.

4.4. Device efficiency

Ideally one would desire the power delivered to the device to be entirely dissipated in the plasma. In reality, however, a finite amount of power is always lost by ohmic heating and by the dielectric loss of the device itself. Following a similar procedure to that in [16], the efficiency of the device in delivering the power from the input port to the plasma can be estimated. The general description of the derivation is outlined here. The input power at the input port divides into two waves, one heading towards the shorted end of the resonator and another one towards the plasma. Assuming that the short is ideal, the incident wave is fully reflected and sent towards the plasma as well. When this reflected wave reaches the plasma, part of it is transmitted to the plasma and part is re-reflected. The re-reflected part is transmitted through the CTLR to the shorted end and reflected again back towards the plasma. Accounting for the fact that the waves attenuate as they transit along the resonator and the infinite number of reflections that take place, the power coupled to the plasma P_{plasma} can be shown to be

$$P_{\text{plasma}} = \frac{1}{2} P_{\text{in}} \left(\mathrm{e}^{-2\alpha l_1} \mathrm{e}^{-2\alpha L} + \mathrm{e}^{-2\alpha l_2} \right) \frac{1 - |\Gamma|^2}{1 - |\Gamma|^2 \mathrm{e}^{-4\alpha L}}, \quad (7)$$

where P_{in} is the input power available at the input port and $\Gamma = (Z_{\text{p}} - Z_0)/(Z_{\text{p}} + Z_0)$ is the reflection coefficient at the CTLR-plasma interface. Therefore, the efficiency of the device is given by

$$\eta_{\text{CTLR}} = \frac{P_{\text{plasma}}}{P_{\text{in}}} \approx \frac{\left(1 - |\Gamma|^2\right) \mathrm{e}^{-\frac{\pi}{2Q}}}{1 - |\Gamma|^2 \mathrm{e}^{-\frac{\pi}{Q}}}, \quad (8)$$

where we have used $Q = \pi/(\alpha\lambda)$, $L = \lambda/4$ and $l_1 \ll l_2$. Equation (8) indicates that both the quality factor of the resonator and the matching between the characteristic impedance of the resonator and the plasma impedance are important for an efficient transfer of the input power into the plasma. Using equation (8), the device efficiency is ∼54% and ∼83% for the 1 W argon and helium atmospheric-pressure discharges, respectively. The device showed no sign of deterioration after 8 h of continuous operation and has now been operated for months with no visible damage.

4.5. Nonthermal discharge

Ideally, for the treatment of temperature sensitive materials or biological samples, the plasma should not be in thermal equilibrium. The lack of erosion and thermal damage after the operation of the device suggests that the plasma discharge from the CTLR source is far from thermodynamic equilibrium, so the devices described here appear to meet this requirement. In addition, the temperature of the discharge can be estimated by measuring the rotational temperature of molecular impurities present in the discharge. Using the experimental setup described in section 3, the optical emission of a 1.5 W argon (15 slm) plasma open to the air was recorded (figure 9). Using LIFBASE [27], the rotational temperature of the OH band at 309 nm was estimated to be ∼400 K. This result agrees with the rotational temperature of N_2 measured in similar microwave-induced atmospheric-pressure plasmas [28, 29]. Generating a Boltzmann plot, the excitation temperature T_{exc} at 4 W input power and 3 slm gas flow rate is determined as being ∼0.45 eV, which based on the results of a collisional–radiative model of an atmospheric-pressure argon discharge [29], suggests that the electron temperature T_{e} is ∼1.8 eV. The large difference between the excitation and rotational temperatures highlights the nonthermal character of the discharge.

5. Conclusion

We have designed, fabricated and characterized microwave-excited microplasma sources based on a CTLR. The devices

are capable of sustaining discharges in argon and helium in a wide pressure range, including atmospheric pressure. We reported two devices, one that operates at 2.45 GHz and one that operates at 900 MHz. Different dielectric materials have been used, and, in particular, the 900 MHz device was built with air as a dielectric. This allowed buffer gases to flow along the resonator, resulting in the formation of a plasma jet at the tip of the device. The devices have a pen-like shape and are suitable for hand-held applications. Because they operate at resonance, no matching network is needed. This eliminates the need for additional components and the associated power losses.

The discharges can be self-ignited with low power and the required breakdown voltage is lower than in dc devices. Once ignited, the device efficiency in transferring the input power into the plasma at atmospheric pressure is 50–85% depending on the gas used. The plasmas generated by these devices are far from thermodynamic equilibrium; based on the rotational temperature of the OH band at 309 nm, their gas temperature is estimated to be ∼400 K. No thermal damage or erosion of the devices was observed, and the plasma jets created can be touched without feeling any thermal effect. In addition, we reported estimates of the plasma density, excitation temperature, electron density and electron temperature based on plasma impedance measurements, the analysis of the optical emission spectrum and the Mach–Zehnder interferometer method.

These characteristics make the CTLR plasma sources attractive for biomedical applications such as treatment of living cell and sterilization of instruments.

Acknowledgments

This work was supported by the Korea Science and Engineering Foundation (KOSEF) grant funded by the Korea government (MOST) (No R01-2007-000-10730-0) and the Korea Ministry of Education, Science, and Technology through its Brain Korea 21 program.

References

[1] Iza F, Kim G J, Lee S M, Lee J K, Walsh J L, Zhang Y T and Kong M G 2008 Microplasmas: Sources, Particle Kinetics, and Biomedical Applications *Plasma Process. Polym.* **5** 322–44

[2] Dudek D, Bibinov N, Engemann J and Awakowicz P 2007 Direct current plasma jet needle source *J. Phys. D: Appl. Phys.* **40** 7367–71

[3] Mohamed A-A H, Block R and Schoenbach K H 2002 Direct Current Glow Discharge in Atmospheric Air *IEEE Trans. Plasma Sci.* **30** 182–3

[4] Fridman G, Shereshevsky A, Jost M M, Brooks A D, Fridman A, Gutsol A, Vasilets V and Friedman G 2007 Floating Electrode Dielectric Barrier Discharge Plasma in Air Promoting Apoptotic Behavior in Melanoma Skin Cancer Cell Lines *Plasma Chem. Plasma Process* **27** 163–76

[5] Park J, Henins I, Herrmann H W, Selwyn G S, Jeong J Y, Hicks R F, Shim D and Chang C S 2000 An atmospheric-pressure plasma source *Appl. Phys. Lett.* **76** 288

[6] Schulz-von der Gathen V, Schaper L, Knake N, Reuter S, Niemi K, Gans T and Winter J 2008 Spatially resolved diagnostics on a microscale atmospheric pressure plasma jet *J. Phys. D: Appl. Phys.* **41** 194004

[7] Stoffels E, Flikweert A J, Stoffels W W and Kroesen G M W 2002 Plasma needle: a non-destructive atmospheric plasma source for fine surface treatment of (bio)materials *Plasma Sources Sci. Technol.* **11** 383–8

[8] Iza F and Hopwood J A 2003 Low-power microwave plasma source based on a microstrip split-ring resonator *IEEE Trans. Plasma Sci.* **31** 782–7

[9] Gesche R, Kühn S and Andrei C 2008 Plasma ignition in a quarter-wavelength microwave slot resonator *J. Phys. D: Appl. Phys.* **41** 194003

[10] Stonies R, Schermer S, Voges E and Broekaert J A C 2004 A new small microwave plasma torch *Plasma Sources Sci. Technol.* **13** 604–11

[11] Walsh J L and Kong M G 2007 Room-temperature atmospheric argon plasma jet sustained with submicrosecond high-voltage pulses *Appl. Phys. Lett.* **91** 221502

[12] Park B J, Lee D H, Park J C, Lee I S, Lee K Y, Hyun S O, Chun M S and Chung K H 2003 Sterilization using a microwave-induced argon plasma system at atmospheric pressure *Phys. Plasmas* **10** 4539–44

[13] Uhm H S, Cho S C, Hong Y C, Park Y G and Park J S 2008 Destruction of dimethyl methylphosphonate using a microwave plasma torch *Appl. Phys. Lett.* **92** 071503

[14] Kuo S P, Popovic S, Tarasenko O, Rubinraut M and Raskovic M 2007 Fan-shaped microwave plasma for mail decontamination *Plasma Sources Sci. Technol.* **16** 581–6

[15] Lai W, Lai H, Kuo S P, Tarasenko O and Levon K 2005 Decontamination of biological warfare agents by a microwave plasma torch *Phys. Plasmas* **12** 023501

[16] Iza F and Hopwood J 2005 Split-ring resonator microplasma: microwave model, plasma impedance and power efficiency *Plasma Sources Sci. Technol.* **14** 397–406

[17] Choi J, Iza F, Lee J K and Ryu C-M 2007 Electron and ion kinetics in a DC microplasma at atmospheric pressure *IEEE Trans. Plasma Sci.* **35** 1274–8

[18] Iza F, Lee J K and Kong M G 2007 Electron kinetics in radio-frequency atmospheric-pressure microplasmas *Phys. Rev. Lett.* **99** 075004

[19] Hong Y J, Lee S M, Kim G C and Lee J K 2008 Modeling high-pressure microplasmas: comparison of fluid modeling and particle-in-cell Monte Carlo collision modeling *Plasma Process. Polym.* **5** 583–92

[20] Hong Y J, Yoon M, Iza F, Kim G C and Lee J K 2008 Comparison of fluid and particle-in-cell simulations on atmospheric pressure helium microdischarges *J. Phys. D: Appl. Phys.* **41** 245208

[21] Pozar D M 2005 *Microwave Engineering* 3rd edn. (New York: Wiley) chapter 2

[22] Lieberman M A and Lichtenberg A J 2005 *Principles of Plasma Discharges and Materials Processing* 2nd edn (New York: Wiley) p 80

[23] Iza F 2004 Atmospheric microplasma source based on a microstrip split-ring resonator *PhD Thesis* Northeastern University

[24] Wilson C G, Gianchandani Y B and Wendt A E 2003 High-voltage constraints for vacuum packaged microstructures *J. Microelectromech. Syst.* **12** 835–9

[25] Meek J M and Craggs J D 1978 *Electrical Breakdown of Gases* (New York: Wiley) p 697

[26] Hopwood J, Iza F, Coy S and Fenner D B 2005 A microfabricated atmospheric-pressure microplasma source operating in air *J. Phys. D: Appl. Phys.* **38** 1698–703

[27] http://www.sri.com/psd/lifbase/

[28] Iza F and Hopwood J A 2004 Rotational, vibrational, and excitation temperatures of a microwave-frequency microplasma *IEEE Trans. Plasma Sci.* **32** 498–504

[29] Zhu X, Chen W and Pu Y K 2008 Gas temperature, electron density and electron temperature measurement in a microwave excited microplasma *J. Phys. D: Appl. Phys.* **41** 105212

[30] Leipold F, Stark R H, El-Habachi A and Schoenbach K H 2000 Electron density measurements in an atmospheric pressure air plasma by means of infrared heterodyne interferometry *J. Phys. D: Appl. Phys.* **33** 2268–73